Nano Research
2024, 17(7): 6119–6126

ISSN 1998-0124 CN 11-5974/O4
https://doi.org/10.1007/s12274-024-6592-7

Research Article

A bifunctional nitrile additive for high-performance lithium-oxygen batteries

Ziwei Li[1,2], Yue Yu[3], Dongyue Yang[2,4], Jin Wang[2], Junmin Yan[1], Gang Huang[2,4], Tong Liu[2,4] (✉), and Xinbo Zhang[2,4] (✉)

[1] *Key Laboratory of Automobile Materials, Ministry of Education, Department of Materials Science and Engineering, Jilin University, Changchun 130022, China*
[2] *State Key Laboratory of Rare Earth Resource Utilization, Changchun Institute of Applied Chemistry, Chinese Academy of Sciences, Changchun 130022, China*
[3] *Department of Chemistry and Waterloo Institute for Nanotechnology, University of Waterloo, 200 University Ave. W., Waterloo, Ontario N2L 3G1, Canada*
[4] *School of Applied Chemistry and Engineering, University of Science and Technology of China, Hefei 230026, China*

© Tsinghua University Press 2024

Received: 15 January 2024 / **Revised:** 26 February 2024 / **Accepted:** 26 February 2024

ABSTRACT

Li-O_2 batteries with high energy density hold significant promise as next-generation energy storage systems. However, Li-O_2 batteries have poor cycling performance at high current densities and large capacities, primarily due to the high impedance caused by the instability of the lithium anode and the sluggish kinetics in the discharge products decomposition on the cathode. Herein, we investigated a bifunctional nitrile additive (2-methoxy benzonitrile (2-MBN)) with good chemical/electrochemical stability to improve the performances of Li-O_2 batteries. The 2-MBN could actively modify the anode by ensuring uniform Li^+ deposition and optimizing the composition of solid electrolyte interphase (SEI). Meanwhile, it could also facilitate the decomposition of discharge products by inducing the formation of sheet-like Li_2O_2, significantly reducing the battery charge overpotential. The bifunctional effects of 2-MBN for the anode and cathode enable Li-O_2 batteries to achieve a stable lifetime of 97 cycles at a current density of 600 mA·g^{-1} with a fixed capacity of 2000 mAh·g^{-1}, much better than that of Li-O_2 batteries without 2-MBN (28 cycles). The inclusion of 2-MBN provides an effective approach for attaining high-performance Li-O_2 batteries.

KEYWORDS

nitrile additives, Li-O_2 batteries, lithium metal anode, charge overpotential

1 Introduction

Lithium-oxygen (Li-O_2) batteries are renowned for their impressive theoretical energy density of 3500 Wh·kg^{-1}, which facilitates to overcome the inherent limitations of traditional lithium-ion batteries (~ 350 Wh·kg^{-1}) [1, 2]. However, the extensively researched nonaqueous Li-O_2 batteries have limited cycling performance at high current densities and large capacities, which severely restricts their application. The limitations could be attributed to the crucial challenges encountered by anodes and cathodes. The uneven concentration distribution and deposition differences of Li^+ on the anode lead to the formation of internal porous structures, triggering sustained parasitic reactions and leading to a persistent loss of active lithium and electrolytes [3]. Consequently, it results in a significant increase in interfacial impedance [4]. Meanwhile, the discharge product with low conductivity, Li_2O_2, accumulates on the cathode, gradually causing electrode passivation. Therefore, the difficulty in product decomposition not only reduces energy conversion efficiency but also generates by-products, thereby shortening the battery cycle life [5].

To enhance the comprehensive performance of Li-O_2 batteries, numerous strategies have been proposed. For the anode, developing artificial or *in-situ* solid electrolyte interphase (SEI) can inhibit parasitic reaction at the interface, and constructing three-dimensional (3D) structural configurations for lithium anodes can promote uniform deposition of lithium ions [6–8]. For the cathode, optimizing compositions and structures can improve the efficiency of oxygen chemical reaction, and adjusting electrolyte composition can alter the reaction path of Li_2O_2, thereby enhancing the reversible decomposition of Li_2O_2 [9–13]. However, it is noteworthy that most optimization strategies for anodes and cathodes are implemented independently, which raises process complexity and compatibility challenges. As the crucial bridge between the cathode and anode, electrolyte plays a vital role in the battery, in which the design of multifunctional additives is emerging as a promising method. In Li-O_2 batteries, additives can optimize the composition of SEI by beneficial priority decomposition and serve as redox mediators or oxygen shuttles to facilitate the reactive activity towards oxygen reduction reaction/oxygen evolution reaction (ORR/OER) [14, 15]. Nevertheless, the consumption of various additives during chemical/electrochemical reactions, resulting in a rapid degradation in their effectiveness, cannot be overlooked [16].

Address correspondence to Tong Liu, tongliu@ciac.ac.cn; Xinbo Zhang, xbzhang@ciac.ac.cn

In this work, we employed 2-methoxy benzonitrile (2-MBN) to boost the performance of Li-O_2 batteries. The 2-MBN could exhibit comprehensive stability as a bifunctional additive in Li-O_2 batteries. Structurally, the cyano group of 2-MBN lacks unstable α-H which is easy for nucleophilic attack by superoxide radical anions, demonstrating unique stability in Li-O_2 batteries [17]. Moreover, the methoxy group in 2-MBN possesses the electronic shielding effect, consequently reducing its reactivity with lithium metal. In terms of regulation on the Li anode, the participation of 2-MBN decreases the Li^+ activation energy and improves Li^+ migration, which promotes uniform Li^+ deposition [18, 19]. During the battery cycle, the 2-MBN could also optimize the inner components of the SEI by increasing the content of lithium nitride. On the cathode, the 2-MBN effectively regulates the formation of sheet-like Li_2O_2, which significantly facilitates the discharge product decomposition during the charging process, resulting in a high energy efficiency even at high current densities. Thanks to the bifunctional effects of 2-MBN, Li-O_2 batteries display 97 cycles at a current density of 600 mA·g^{-1} with a fixed capacity of 2000 mAh·g^{-1}. Furthermore, when coupled with the Ru decorated Super P (Ru/SP) catalyst, Li-O_2 batteries with 2-MBN can normally run for 54 cycles at 2500 mA·g^{-1} and 5000 mAh·g^{-1}. As a result, the incorporation of 2-MBN into the electrolyte increases the long-cycling stability of Li-O_2 batteries at high current densities and large capacities.

2 Experimental

2.1 Materials

The following materials were obtained from Aladdin Reagent: dimethyl sulfoxide (DMSO), N-methyl-2-pyrrolidone (NMP), potassium superoxide (KO_2), 2-MBN, benzonitrile (BN), and lithium bis(trifluoromethanesulphonyl)imide (LiTFSI). The lithium chip was obtained from China Energy Lithium Industry Co., Ltd. All the chemical materials were stored in the argon-filled glove box. In addition, the carbon paper was purchased from Phychemi Co., Ltd., and SP was obtained from HF-Kejing Material Technology Co., Ltd. To prepare the electrolyte, lithium salt was dried under vacuum at 120 °C using a Buchi vacuum oven. All solvents were purified with a 4 Å molecular sieve.

2.2 Battery assembly

To prepare the cathode of Li-O_2 batteries, the Super P or ruthenium-based material was mixed with polyvinylidene fluoride (PVDF) binder in NMP at a ratio of 9:1 and coated onto carbon paper. The slurry-coated carbon paper was then dried at 70 °C and stored in an Ar-filled glove box (< 0.1 ppm O_2 and H_2O). The mass loading of active material was 0.1 mg·cm^{-2} in respective test. A standard Li-O_2 coin cell was assembled with a cathode, a glass fiber separator absorbing the DMSO or DMSO/2-MBN electrolyte, and a lithium metal anode. The electrolyte used in the experiment was prepared by dissolving 1 M LiTFSI in DMSO. For comparison, 2-MBN was mixed with DMSO (1:49 v/v) to prepare 1 M LiTFSI in DMSO/2-MBN. Fresh lithium chips were used to confirm the stability of solvents with lithium metal. Meanwhile, before battery cycling, all lithium chips were pre-treated with fluoroethylene carbonate (FEC) to form an initial protection layer. Lithium chips were immersed in FEC for 30 min, cleaned with a lint-free wipe, and dried at room temperature.

2.3 Characterizations

Hitachi S4800 field emission scanning electron microscope analyzer was used for scanning electron microscopy (SEM) characterization to analyze the morphology of the cathode and anode. The X-ray photoelectron spectroscopy (XPS) data was obtained using a vacuum chamber on the ThermoFisher XPS Escalab. The Bruker Avance II 400 spectrometer was used to conduct the nuclear magnetic resonance (NMR) test. A Bruker D8 focused powder X-ray diffractometer was used to perform power X-ray diffraction (XRD) at 40 kV and 40 mA. The Beijing Purkinje General, TU-1900 was used to measure the absorbance spectrum of the ultraviolet–visible (UV–vis) spectrometer.

3 Results and discussion

Avoiding parasitic reactions between nitrile additives and lithium metal is essential for achieving battery stability. The activity of cyano group on 2-MBN is weaker than that of BN. Specifically, the ortho-methoxy group on the benzene ring heightens electron shielding effect on the cyano group, leading to a decrease in acidity of 2-MBN. One-electron reduction reaction between nitrile and lithium metal generates orange-red free radicals [20, 21]. Therefore, the degree of the parasitic reaction between lithium metal and solvents (DMSO, BN, and 2-MBN) can be visually observed based on the color changes (Fig. S1 in the Electronic Supplementary Material (ESM)). As depicted in Figs. 1(a) and 1(b), UV–vis tests were performed on the BN and 2-MBN solutions before and after the reaction with lithium metal. There is a characteristic absorption peak of the BN, associated with anionic radicals related to electron transfer [22], indicating its instability with lithium metal [23]. In contrast, a slight change in the absorption peak of the 2-MBN indicates its low reactivity with lithium metal. Furthermore, the BN was found to form numerous by-products after a week, while the 2-MBN exhibits only a few by-products presenting long-term stability with lithium metal (Fig. S2 in the ESM). To further investigate the corrosion degree of lithium metal in different solvents, the microscopic surface morphology of the lithium chips after soaking in three kinds of solvents was observed by SEM (Figs. 1(c)–1(e)). The overall surface of the lithium chip appears flat in DMSO and 2-MBN. Nevertheless, the lithium chip in BN displays a rough and uneven morphology. All the above tests support the high compatibility of 2-MBN with lithium metal. Given that the reactive oxygen species (ROS) could attack additives and cause rapid chemical degradation during battery operation [24], NMR spectra were performed to verify the 2-MBN stability towards ROS (Fig. 1(f)). The characteristic peaks of 2-MBN remained unchanged when mixed with different oxygen species, reflecting its good stability [25]. Cyclic voltammetry (CV) tests confirm the relative electrochemical stability of both 2-MBN and DMSO electrolytes in the Ar atmosphere (Fig. S3 in the ESM). In O_2, DMSO/2-MBN electrolyte exhibits typical ORR/OER responses for lithium-oxygen electrochemical reactions [26], rather than other electrochemical parasitic reactions [27, 28]. The above stability tests all indicate favorable applicability of 2-MBN in Li-O_2 batteries [17].

To investigate the regulation effect of 2-MBN on lithium metal during cycling, Li/Li symmetric batteries with DMSO or DMSO/2-MBN were tested at current densities of 0.1 and 0.3 mA·cm^{-2} (Fig. S4 in the ESM). As depicted in Fig. 2(a), the Li/Li symmetric battery demonstrates excellent long-term stability for over 380 h with 2-MBN at a current density of 0.1 mA·cm^{-2}, while the battery without 2-MBN shows significant voltage fluctuations after only 90 h, which might be attributed to the continuous accumulation of unstable passivation layer on lithium metal caused by electrolyte decomposition [29]. In addition, the overall impedance of the battery with 2-MBN after 40 cycles is much lower than that of the battery without 2-MBN (Fig. 2(b)). The significant increase in battery impedance without 2-MBN might be mainly due to

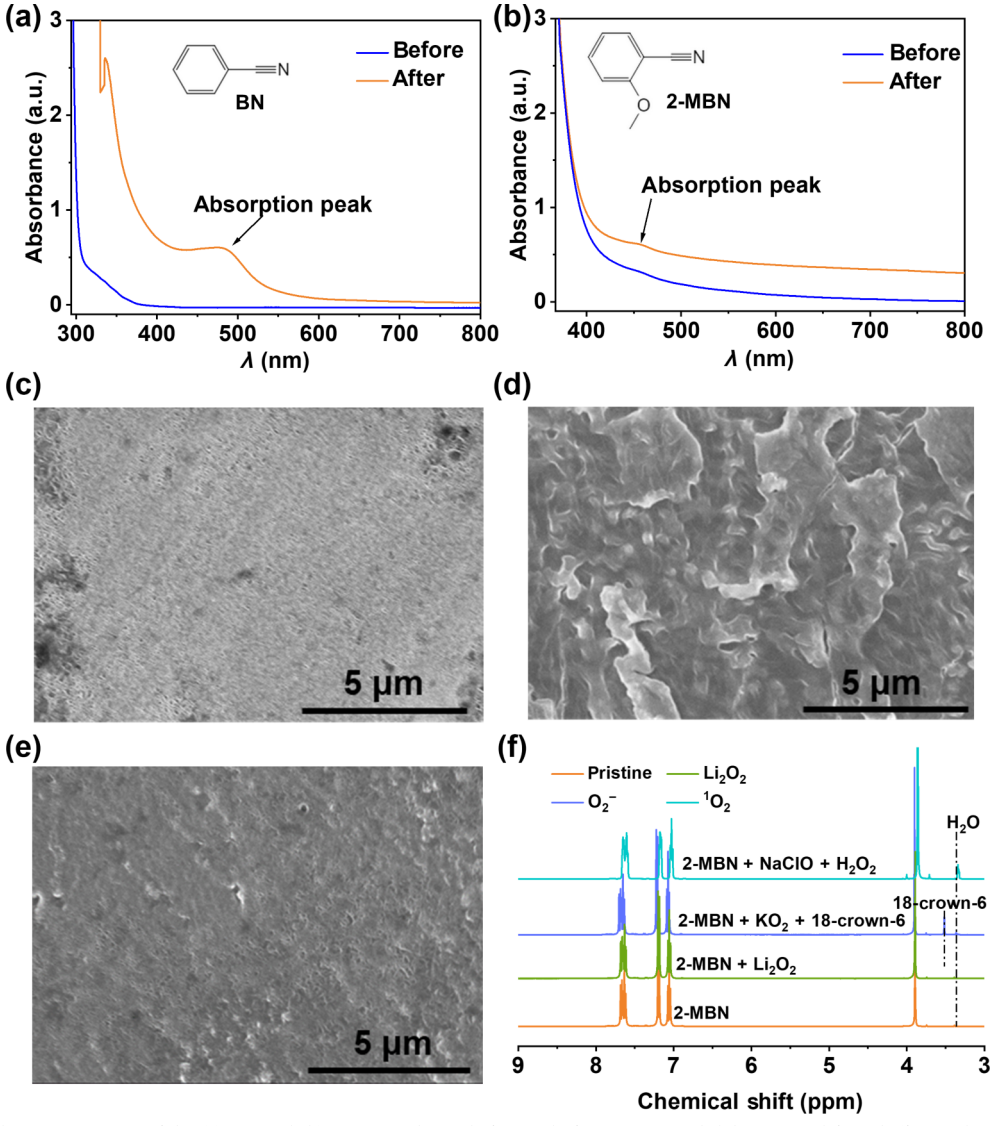

Figure 1 UV–vis absorption spectra of the (a) BN and (b) 2-MBN solvents before and after reacting with lithium metal for 8 h (λ: wavelength). SEM images of lithium surface morphology after soaking in three solvents of (c) the DMSO, (d) BN, and (e) 2-MBN for 8 h. (f) ^{1}H NMR spectra of the 2-MBN solvent with lithium peroxide, superoxide anion, and singlet oxygen.

uneven stripping and deposition of Li^+ on lithium anode, which damages the original surface protective layer and forms the unstable passivation layer on lithium metal, as confirmed by SEM [30]. Figure 2(c) shows an uneven mossy structure of lithium metal surface after cycling in pristine DMSO electrolyte, while the loosely packed porous structure could exacerbate the parasitic reaction between lithium and electrolyte. In contrast, a more uniform and dense surface morphology of lithium metal was formed in DMSO/2-MBN (Fig. 2(d)). It is noteworthy that introducing 2-MBN could alleviate the strong solvation effect of DMSO that aggravates the uneven deposition of lithium ions on the lithium surface [19, 31]. XPS reveals that certain CN_x compounds from the contribution of cyano group are formed on lithium metal surface in the presence of 2-MBN (Figs. 2(e) and 2(f)), and a moderate amount of CN_x will not have an obvious negative impact on the electrode interface [32, 33]. CN_x compounds decrease significantly after Ar ion sputtering, and the inner SEI mainly contains lithium nitride, indicating that the sustained reactions of CN_x are further effectively suppressed by high-quality SEI films (Figs. 2(g) and 2(h)). Li_3N is a well-known fast Li^+ conductor and exhibits excellent stability with lithium metal, which promotes the transmission of Li^+ in SEI. The SEI component after sputtering indicates that the inclusion of 2-MBN helps adjust the composition of passivation layer, and in particular, 2-MBN could reduce organic lithium content and increase lithium nitride content [33]. Meanwhile, the substantial amount of lithium fluoride on lithium surface in both DMSO and DMSO/2-MBN can be attributed to the initial protective layer and lithium salt decomposition during battery cycling (Fig. S5 in the ESM) [29]. Lithium fluoride is considered as an important component of a high-quality SEI, and the presence of moderate CN_x polar group on the SEI surface might be beneficial for breaking C–F bonds in lithium salts, leading to the further formation of lithium fluoride [34–36]. When increasing the current density to 0.3 mA·cm^{-2}, the symmetric battery with DMSO/2-MBN still exhibits a lifespan twice as long as the battery with DMSO, and the component adjustment of 2-MBN on lithium metal surface is similar to that at 0.1 mA·cm^{-2} (Figs. S6–S8 in the ESM). Based on the results of SEM, EIS, and XPS tests, 2-MBN is beneficial for forming and maintaining a uniform and dense SEI, effectively suppressing further parasitic reactions on the lithium metal and decreasing the battery impedance. Therefore, 2-MBN effectively improves the compatibility of DMSO-based electrolytes with lithium metal electrodes.

The effect of 2-MBN in the decomposition of discharge products on cathode has also been studied. As shown in Fig. 3(a), XRD curve of discharged SP cathode displays typical Li_2O_2 peaks, without other obvious by-product peak, which confirms the

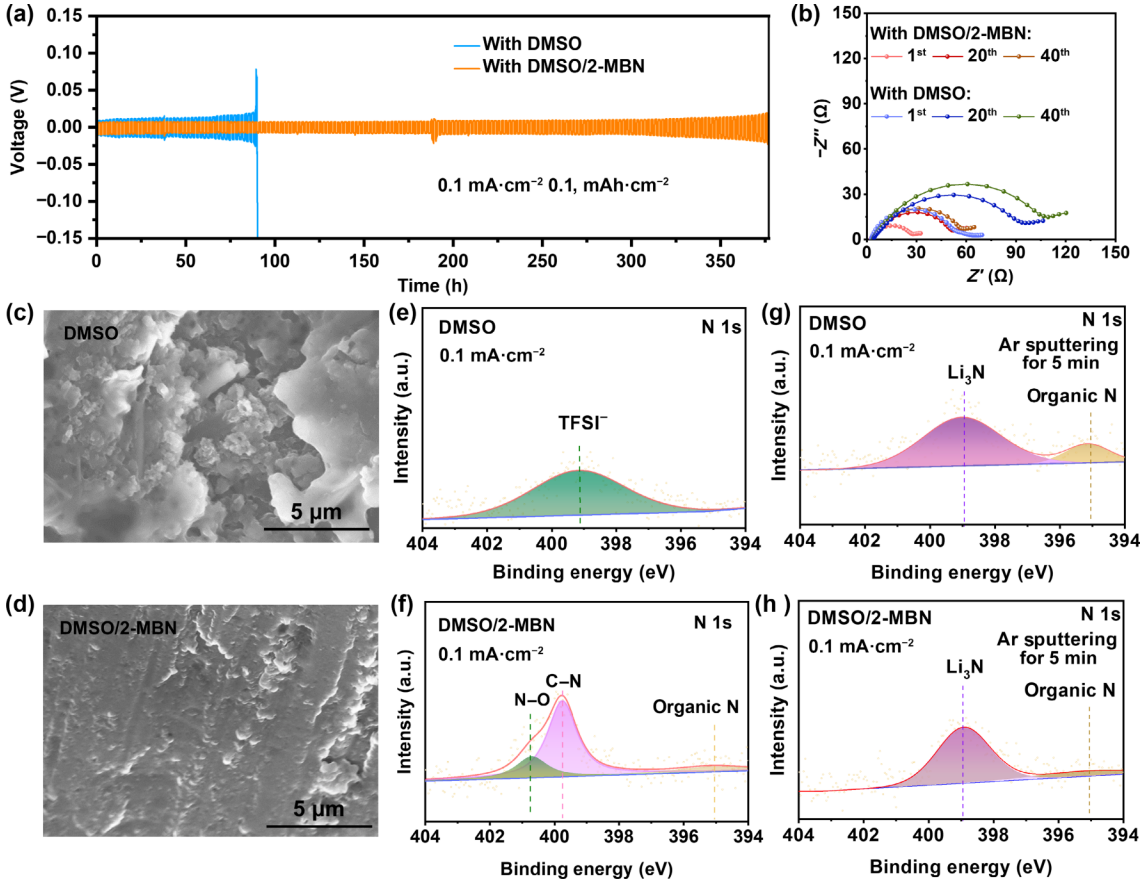

Figure 2 (a) Voltage profiles and (b) impedance spectra of Li/Li symmetric batteries with DMSO or DMSO/2-MBN at a current density of 0.1 mA·cm^{-2}. SEM images of lithium after batteries cycling at 0.1 mA·cm^{-2} with (c) DMSO and (d) DMSO/2-MBN. N 1s XPS spectra of lithium foil after battery cycling at 0.1 mA·cm^{-2} with (e) DMSO and (f) DMSO/2-MBN, and the corresponding spectra of lithium foil with (g) DMSO and (h) DMSO/2-MBN after Ar ion sputtering for 5 min.

stability of the cathode. It should be noted that the sheet-like morphology of discharge products (Li_2O_2) is significantly different from the bulk-like morphology of degradation by-products (LiOH) [37, 38]. In addition, the morphology of sheet-like Li_2O_2 is similar to the reported amorphous Li_2O_2 [11, 39], and the different crystallinity, geometric shape, and size of discharge products have a significant impact on the mass transfer rate [40, 41]. As depicted in Figs. 3(b)–3(d), sheet-like Li_2O_2 formed on the cathode after discharge, which is different from typical solution-mediated Li_2O_2 in DMSO (Fig. S9 in the ESM). The sheet-like Li_2O_2 favors the rapid decomposition, resulting in low charge overpotential and high-rate performance of Li-O_2 batteries [42]. To further investigate the reversible decomposition of discharge product in the battery, differential electrochemical mass spectrometry (DEMS) analysis was conducted on the charging process of the cathode which had discharged with a large limited capacity of 3000 mAh·g^{-1} (Figs. 3(e) and 3(f)). For the cathode in DMSO-based electrolyte, the voltage plateau quickly rises to nearly 4 V, accompanied by a significant release of oxygen. At the end of charging process, the charging plateau rises steeply with a decrease in the amount of released O_2 and a notable increase in the release of CO_2. In contrast, the battery with DMSO/2-MBN maintains a stable charging plateau below 3.9 V throughout the charging process with a vigorous release of O_2 and less release of CO_2. Despite a slight increase in the charge potential under high-capacity conditions, the battery with DMSO/2-MBN still demonstrates superior OER performance [43]. The above results indicate that 2-MBN regulates the formation of Li_2O_2 during discharging process, thereby effectively promoting decomposition of product at low potential, which could improve the battery cycling performance.

The promotion of Li^+ transport plays a crucial role in regulating interfacial reactions. An appropriate amount of 2-MBN promotes the migration of Li^+, resulting in higher Li^+ conductivity of the electrolyte compared to DMSO electrolyte, which is also beneficial for inhibiting the dendritic growth of Li (Fig. 4(a)) [35]. The activation energy of DMSO/2-MBN electrolyte is less than the DMSO electrolyte (5.85 vs. 6.03 kJ·mol^{-1}), suggesting the improvement in the Li^+ migration kinetic (Fig. 4(b)). Meanwhile, it can be seen that the ionic conductivities of the DMSO/2-MBN are always higher than those of DMSO electrolyte at the same temperature. Better Li^+ migration ability in DMSO/2-MBN electrolytes is also supported by the increased lithium-ion transfer number of 0.54, which is higher than the 0.49 of pristine DMSO electrolytes (Fig. 4(c) and Fig. S10 in the ESM). The Li^+ electron cloud density is affected by the combined strength of anion and solvent. High donor number (DN) solvents like DMSO significantly affect the coordination of lithium ions, for the strong solvation effect of DMSO on Li^+ results in relatively less free Li^+ exposure [44]. In contrast, the competitive coordination of solvents can promote the de-solvation of lithium ions [45]. The inclusion of 2-MBN leads to a shift in the ^{7}Li peak to a lower field, indicating weakened overall solvation effects (Fig. 4(d)) [46]. During the discharging process on the cathode, the retention capacity of the LiO_2 intermediate in the solvent directly affects the discharge path [47]. The promotion of Li^+ migration also increases the binding rate of $Li^+_{(sol)}$ and $O_{2(sol)}$ on the cathode, facilitating the dissociation equilibrium to shift towards the formation of $LiO_{2(sol)}$, which will promote the transition in Li_2O_2 morphology [39, 48]. Therefore, Li-O_2 batteries with DMSO/2-MBN have comprehensive advantages in balancing Li^+ deposition to inhibit lithium dendrites on the anode and improve the decomposition kinetics of cathodic discharge products (Fig. 4(e)).

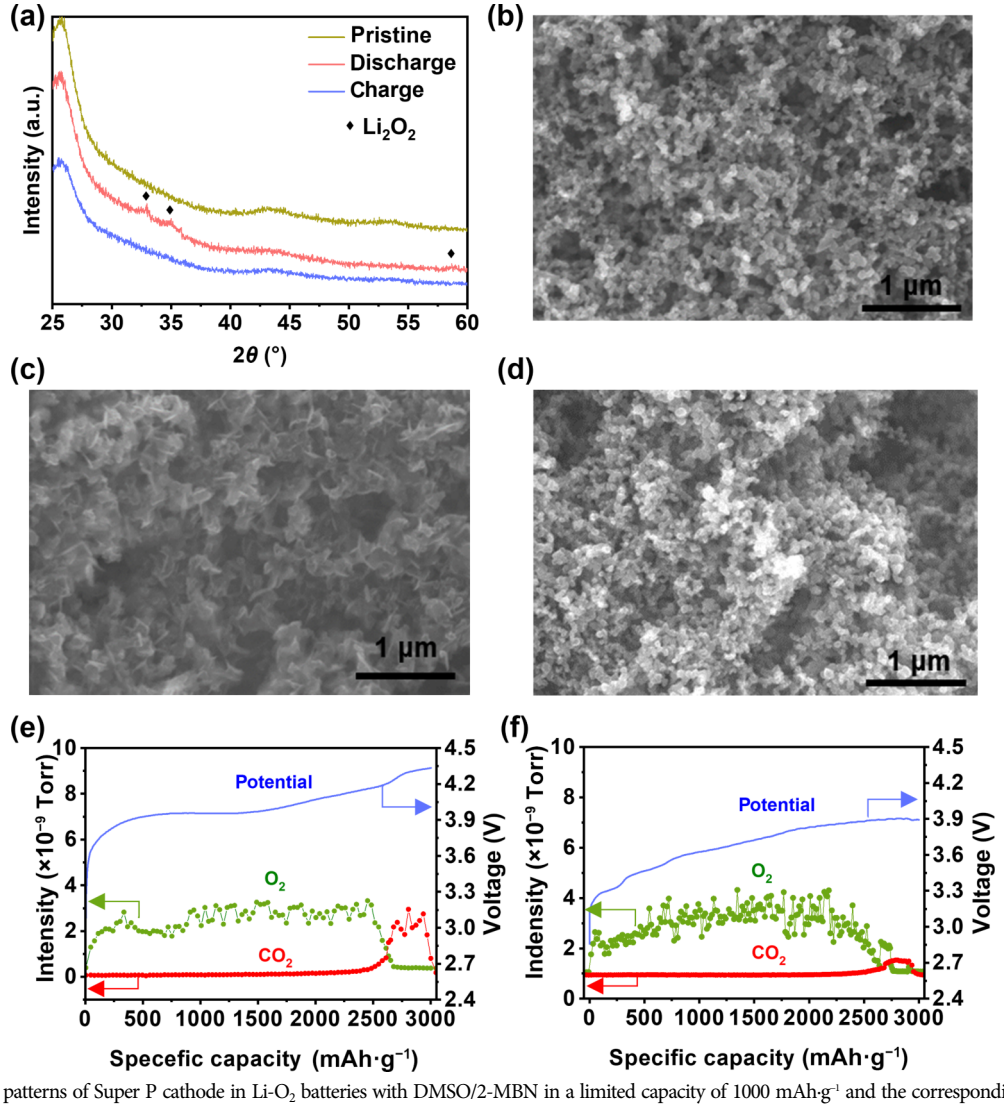

Figure 3 (a) XRD patterns of Super P cathode in Li-O_2 batteries with DMSO/2-MBN in a limited capacity of 1000 mAh·g^{-1} and the corresponding SEM images (b) before discharge, (c) after discharge, and (d) subsequent recharge. DEMS analysis of Li-O_2 batteries with (e) DMSO and (f) DMSO/2-MBN.

The comprehensive effect of 2-MBN on the electrode interfaces can be reflected in the cycling performance of Li-O_2 batteries. Firstly, Super P cathodes were used to compare the impact of intrinsic electrolyte differences on battery performance. The battery with DMSO/2-MBN exhibits a remarkable cycle life of 160 cycles at a current density of 300 mA·g^{-1} with a fixed capacity of 1000 mAh·g^{-1}, while the battery with DMSO only presents a cycle lifetime of 77 cycles (Fig. 5(a) and Fig. S11 in the ESM). Moreover, even at a higher current density of 600 mA·g^{-1} and a higher capacity limitation of 2000 mAh·g^{-1}, the battery with DMSO/2-MBN can still run stably for 97 cycles, which is much more than 28 cycles of the battery with DMSO (Figs. 5(b) and 5(c)). Figure 5(d) shows the comparison of charge and discharge curves for the first cycle of batteries with/without 2-MBN at different current densities, demonstrating the favorable performance of batteries with DMSO/2-MBN. Additionally, the full discharge–charge test reveals that the charge potential of a battery with DMSO/2-MBN remains much lower than that of a battery without 2-MBN (Fig. 5(e)). Since suitable cathode catalyst can further optimize the battery cycling performance at high current density and large capacity, Ru/SP cathode was then coupled with DMSO/2-MBN electrolyte [49–51]. It is clear that even at a much higher current density of 2500 mA·g^{-1} and a cut-off capacity of 5000 mAh·g^{-1}, the battery with DMSO/2-MBN can still run for 54 cycles, 2 times higher than that of the battery without 2-MBN (Fig. 5(f) and Fig. S12 in the ESM). The above tests indicate that 2-MBN exactly plays a positive role in boosting the battery lifetime and can satisfy the fast charge transfer kinetics requirement for cycling Li-O_2 batteries at high rates and large capacities.

4 Conclusions

In conclusion, a bifunctional nitrile additive (2-MBN) has been researched to enhance the performance of Li-O_2 batteries. The 2-MBN exhibits high stability towards reactive oxygen species and lithium metal. Specifically, the 2-MBN improves the migration ability of Li^+, thereby facilitating the uniform deposition of Li^+ on the lithium metal surface. Meanwhile, it optimizes the composition of inner SEI by increasing the content of Li_3N. On the other hand, the 2-MBN regulates the formation and promotes effective decomposition of Li_2O_2 on the cathode, which significantly reduces the battery charging overpotential. The comprehensive effects of 2-MBN prolong the cycling performance of Li-O_2 batteries at high current densities and large capacities. The 2-MBN possesses high application potential and could cooperate with other optimized approaches to promote further exploration in Li-O_2 batteries.

Acknowledgements

This work was financially supported by the National Key R&D Program of China (No. 2019YFA0705700), the National Natural

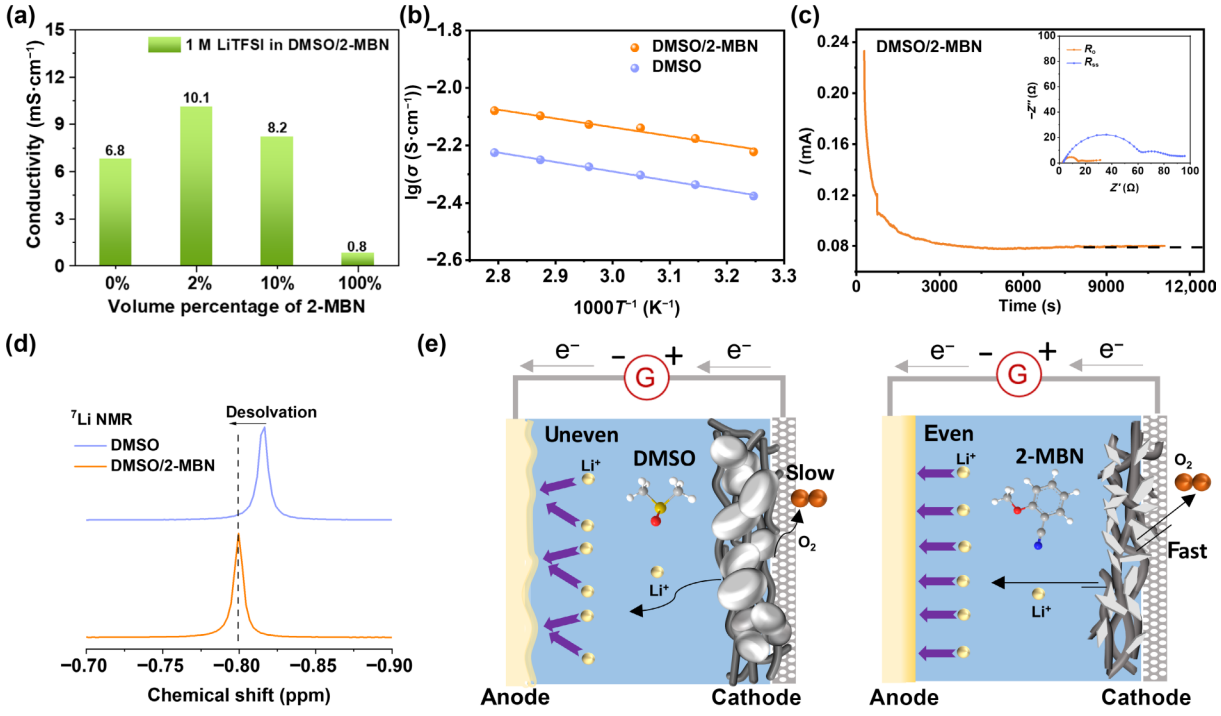

Figure 4 (a) Ionic conductivity in DMSO/2-MBN electrolytes with different volume ratios. (b) Temperature-dependent ionic conductivity plots of different electrolytes. (c) Chronoamperometric curve of the Li/Li symmetric batteries with DMSO/2-MBN electrolyte. Inset is the corresponding EIS curves before and after potentiostatic direct current (DC) polarization. (d) ^{7}Li NMR spectra of 1 M LiTFSI in DMSO and 1 M LiTFSI in DMSO/2-MBN electrolytes. (e) Schematic diagram of the comprehensive effect of 2-MBN on Li-O_2 batteries.

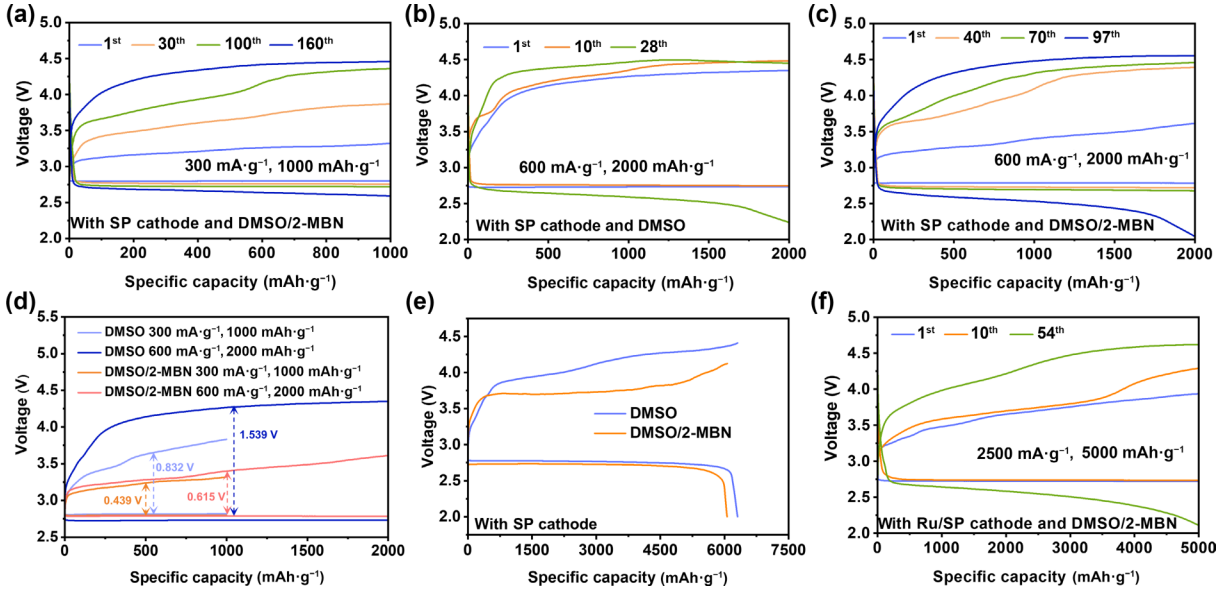

Figure 5 (a) Cycling profiles of Li-O_2 battery with DMSO/2-MBN in a capacity limitation of 1000 mAh·g^{-1} at a current density of 300 mA·g^{-1}. Cycling profiles of Li-O_2 batteries with (b) DMSO and (c) DMSO/2-MBN in a capacity limitation of 2000 mAh·g^{-1} at a current density of 600 mA·g^{-1}. (d) The first discharge/charge curves of Li-O_2 batteries with different electrolytes under different conditions. (e) The full discharge/charge curves of Li-O_2 batteries with different electrolytes. (f) Li-O_2 batteries with Ru/SP and DMSO/2-MBN in a capacity limitation of 5000 mAh·g^{-1} at a current density of 2500 mA·g^{-1}.

Science Foundation of China (Nos. U22A20437, U23A20575, 52171194, 52271140, and 22209138), the CAS Project for Young Scientists in Basic Research (No. YSBR-058), the China Postdoctoral Science Foundation (No. 2022M713070), and the National Natural Science Foundation of China Outstanding Youth Science Foundation of China (Overseas).

Electronic Supplementary Material: Supplementary material (optical images of lithium metal chips, SEM images of discharged cathodes in different electrolytes, XPS spectra of lithium metal foils in different electrolytes, voltage profiles of the Li/Li symmetric batteries, test curves of lithium-oxygen batteries, and electrolyte electrochemical measurements) is available in the online version of this article at https://doi.org/10.1007/s12274-024-6592-7.

References

[1] Aurbach, D.; McCloskey, B. D.; Nazar, L. F.; Bruce, P. G. Advances in understanding mechanisms underpinning lithium-air batteries. *Nat. Energy* **2016**, *1*, 16128.

[2] Farahmandjou, M.; Zhao, S. Q.; Lai, W. H.; Sun, B.; Notten, P. H. L.; Wang, G. X. Oxygen redox chemistry in lithium-rich cathode materials for Li-ion batteries: Understanding from atomic structure to nano-engineering. *Nano Mater. Sci.* **2022**, *4*, 322–338.

[3] Ding, Y. J.; Li, Y. J.; Wu, Z. S. Recent advances and challenges in

the design of Li-air batteries oriented solid-state electrolytes. *Battery Energy* **2023**, *2*, 20220014.
[4] Zhang, J.; Shi, J. Y.; Wen, X. Y.; Zhao, Y. F.; Guo, J. G. Properties of thin lithium metal electrodes in carbonate electrolytes with realistic parameters. *ACS Appl. Mater. Interfaces* **2020**, *12*, 32863–32870.
[5] Liu, T.; Zhao, S. Y.; Xiong, Q.; Yu, J.; Wang, J.; Huang, G.; Ni, M.; Zhang, X. B. Reversible discharge products in Li-air batteries. *Adv. Mater.* **2023**, *35*, 2208925.
[6] Liu, S. J.; Jiao, K. J.; Yan, J. H. Prospective strategies for extending long-term cycling performance of anode-free lithium metal batteries. *Energy Storage Mater.* **2023**, *54*, 689–712.
[7] Zhao, Q.; Stalin, S.; Archer, L. A. Stabilizing metal battery anodes through the design of solid electrolyte interphases. *Joule* **2021**, *5*, 1119–1142.
[8] Zhai, P. B.; Wei, Y.; Xiao, J.; Liu, W.; Zuo, J. H.; Gu, X. K.; Yang, W. W.; Cui, S. Q.; Li, B.; Yang, S. B. et al. *In situ* generation of artificial solid-electrolyte interphases on 3D conducting scaffolds for high-performance lithium-metal anodes. *Adv. Energy Mater.* **2020**, *10*, 1903339
[9] Li, F. J.; Zhang, T.; Zhou, H. S. Challenges of non-aqueous Li-O_2 batteries: Electrolytes, catalysts, and anodes. *Energy Environ. Sci.* **2013**, *6*, 1125–1141.
[10] Yang, Y.; Zhang, T.; Wang, X. C.; Chen, L. F.; Wu, N.; Liu, W.; Lu, H. F.; Xiao, L.; Fu, L.; Zhuang, L. Tuning the morphology and crystal structure of Li_2O_2: A graphene model electrode study for Li-O_2 battery. *ACS Appl. Mater. Interfaces* **2016**, *8*, 21350–21357.
[11] Sun, Z. M.; He, J. L.; Yuan, M. W.; Lin, L.; Zhang, Z.; Kang, Z.; Liao, Q. L.; Li, H. F.; Sun, G. B.; Yang, X. J. et al. Li^+-clipping for edge S-vacancy MoS_2 quantum dots as an efficient bifunctional electrocatalyst enabling discharge growth of amorphous Li_2O_2 film. *Nano Energy* **2019**, *65*, 103996.
[12] Zhang, G. L.; Li, G. Y.; Wang, J.; Tong, H.; Wang, J. C.; Du, Y.; Sun, S. H.; Dang, F. 2D SnSe cathode catalyst featuring an efficient facet-dependent selective Li_2O_2 growth/decomposition for Li-oxygen batteries. *Adv. Energy Mater.* **2022**, *12*, 2103910
[13] Zhang, G. L.; Liu, C. Y.; Guo, L.; Liu, R. W.; Miao, L.; Dang, F. Electronic "bridge" construction via ag intercalation to diminish catalytic anisotropy for 2D Tin diselenide cathode catalyst in lithium-oxygen batteries. *Adv. Energy Mater.* **2022**, *12*, 2200791.
[14] Zhang, J. Q.; Sun, B.; Zhao, Y. F.; Tkacheva, A.; Liu, Z. J.; Yan, K.; Guo, X.; McDonagh, A. M.; Shanmukaraj, D.; Wang, C. Y. et al. A versatile functionalized ionic liquid to boost the solution-mediated performances of lithium-oxygen batteries. *Nat. Commun.* **2019**, *10*, 602.
[15] Wang, D.; Zhang, F.; He, P.; Zhou, H. S. A versatile halide ester enabling Li-anode stability and a high rate capability in lithium-oxygen batteries. *Angew. Chem., Int. Ed.* **2019**, *58*, 2355–2359.
[16] Nakanishi, A.; Thomas, M. L.; Kwon, H. M.; Kobayashi, Y.; Tatara, R.; Ueno, K.; Dokko, K.; Watanabe, M. Electrolyte composition in Li/O_2 batteries with LiI redox mediators: Solvation effects on redox potentials and implications for redox shuttling. *J. Phys. Chem. C* **2018**, *122*, 1522–1534.
[17] Bryantsev, V. S.; Uddin, J.; Giordani, V.; Walker, W.; Addison, D.; Chase, G. V. The identification of stable solvents for nonaqueous rechargeable Li-air batteries. *J. Electrochem. Soc.* **2012**, *160*, A160–A171.
[18] Semino, R.; Zaldivar, G.; Calvo, E. J.; Laria, D. Lithium solvation in dimethyl sulfoxide-acetonitrile mixtures. *J. Chem. Phys.* **2014**, *141*, 214509.
[19] Wu, J. Y.; Li, X. W.; Rao, Z. X.; Xu, X. N.; Cheng, Z. X.; Liao, Y. Q.; Yuan, L. X.; Xie, X. L.; Li, Z.; Huang, Y. H. Electrolyte with boron nitride nanosheets as leveling agent towards dendrite-free lithium metal anodes. *Nano Energy* **2020**, *72*, 104725.
[20] Romanin, A. M.; Gennaro A.; Vianello, E. Electrode reduction mechanism of aromatic nitriles in aprotic solvents: Benzonitrile. *J. Electroanal. Chem.* **1978**, *88*, 175–185.
[21] Rieger, P. H.; Bernal, I.; Reinmuth, W. H.; Fraenkel, G. K. Electron spin resonance of electrolytically generated nitrile radicals. *J. Am. Chem. Soc.* **1963**, *85*, 683–693.
[22] Pedersen, S. U.; Christensen, T. B.; Thomasen, T.; Daasbjerg, K. New methods for the accurate determination of extinction and diffusion coefficients of aromatic and heteroaromatic radical anions in N,N-dimethylformamide. *J. Electroanal. Chem.* **1998**, *454*, 123–143.
[23] Lin, X. C.; Li, N.; Zhang, W. J.; Huang, Z. J.; Tang, Q.; Gong, C. B.; Fu, X. K. Synthesis and electrochromic properties of benzonitriles with various chemical structures. *Dyes Pigments* **2019**, *171*, 107783.
[24] Lee, H. W.; Kim, J. Y.; Kim, J. E.; Jo, Y. J.; Dewar, D.; Yang, S. X.; Gao, X. W.; Bruce, P. G.; Kwak, W. J. Effect of singlet oxygen on redox mediators in lithium-oxygen batteries. *J. Mater. Chem. A* **2023**, *11*, 16003–16008.
[25] Xie, J. B.; Bao, J. J.; Li, H. X.; Tan, D. W.; Li, H. Y.; Lang, J. P. An efficient approach to the ammoxidation of alcohols to nitriles and the aerobic oxidation of alcohols to aldehydes in water using Cu(II)/pypzacac complexes as catalysts. *RSC Adv.* **2014**, *4*, 54007–54017.
[26] Zakharchenko, T. K.; Kozmenkova, A. Y.; Isaev, V. V.; Itkis, D. M.; Yashina, L. V. Positive electrode passivation by side discharge products in Li-O_2 batteries. *Langmuir* **2020**, *36*, 8716–8722.
[27] Bondue, C. J.; Hegemann, M.; Molls, C.; Thome, E.; Baltruschat, H. A comprehensive study on oxygen reduction and evolution from lithium containing DMSO based electrolytes at gold electrodes. *J. Electrochem. Soc.* **2016**, *163*, A1765–A1775.
[28] Amin, H. M. A.; Molls, C.; Bawol, P. P.; Baltruschat, H. The impact of solvent properties on the performance of oxygen reduction and evolution in mixed tetraglyme-dimethyl sulfoxide electrolytes for Li-O_2 batteries: Mechanism and stability. *Electrochim. Acta* **2017**, *245*, 967–980.
[29] Lee, H.; Lee, D. J.; Lee, J. N.; Song, J.; Lee, Y.; Ryou, M. H.; Park, J. K.; Lee, Y. M. Chemical aspect of oxygen dissolved in a dimethyl sulfoxide-based electrolyte on lithium metal. *Electrochim. Acta* **2014**, *123*, 419–425.
[30] Wang, M. M.; Cheng, X. P.; Cao, T. C.; Niu, J. J.; Wu, R.; Liu, X. Q.; Zhang, Y. F. Constructing ultrathin TiO_2 protection layers via atomic layer deposition for stable lithium metal anode cycling. *J. Alloys Compd.* **2021**, *865*, 158748.
[31] Smirnov, V. S.; Kislenko, S. A. Effect of solvents on the behavior of lithium and superoxide ions in lithium-oxygen battery electrolytes. *ChemPhysChem* **2018**, *19*, 75–81.
[32] Hellgren, N.; Haasch, R. T.; Schmidt, S.; Hultman, L.; Petrov, I. Interpretation of X-ray photoelectron spectra of carbon-nitride thin films: New insights from *in situ* XPS. *Carbon* **2016**, *108*, 242–252.
[33] Lv, Z. L.; Zhou, Q.; Zhang, S.; Dong, S. M.; Wang, Q. L.; Huang, L.; Chen, K.; Cui, G. L. Cyano-reinforced *in-situ* polymer electrolyte enabling long-life cycling for high-voltage lithium metal batteries. *Energy Storage Mater.* **2021**, *37*, 215–223.
[34] Liu, Y. J.; Tao, X. Y.; Wang, Y.; Jiang, C.; Ma, C.; Sheng, O. W.; Lu, G. X.; Lou, X. W. Self-assembled monolayers direct a LiF-rich interphase toward long-life lithium metal batteries. *Science* **2022**, *375*, 739–745.
[35] Lee, S. H.; Hwang, J. Y.; Park, S. J.; Park, G. T.; Sun, Y. K. Adiponitrile ($C_6H_8N_2$): A new Bi-functional additive for high-performance li-metal batteries. *Adv. Funct. Mater.* **2019**, *29*, 1902496.
[36] Zhang, J. G.; Xu, W.; Xiao, J.; Cao, X.; Liu, J. Lithium metal anodes with nonaqueous electrolytes. *Chem. Rev.* **2020**, *120*, 13312–13348.
[37] Temprano, I.; Liu, T.; Petrucco, E.; Ellison, J. H. J.; Kim, G.; Jónsson, E.; Grey, C. P. Toward reversible and moisture-tolerant aprotic lithium-air batteries. *Joule* **2020**, *4*, 2501–2520.
[38] Kwabi, D. G.; Batcho, T. P.; Amanchukwu, C. V.; Ortiz-Vitoriano, N.; Hammond, P.; Thompson, C. V.; Shao-Horn, Y. Chemical instability of dimethyl sulfoxide in lithium-air batteries. *J. Phys. Chem. Lett.* **2014**, *5*, 2850–2856.
[39] Dutta, A.; Wong, R. A.; Park, W.; Yamanaka, K.; Ohta, T.; Jung, Y.; Byon, H. R. Nanostructuring one-dimensional and amorphous lithium peroxide for high round-trip efficiency in lithium-oxygen batteries. *Nat. Commun.* **2018**, *9*, 680.
[40] Luo, Y. T.; Bai, Y.; Mistry, A.; Zhang, Y. W.; Zhao, D. X.; Sarkar,

S.; Handy, J. V.; Rezaei, S.; Chuang, A. C.; Carrillo, L. et al. Effect of crystallite geometries on electrochemical performance of porous intercalation electrodes by multiscale *operando* investigation. *Nat. Mater.* **2022**, *21*, 217–227.

[41] Tian, F.; Radin, M. D.; Siegel, D. J. Enhanced charge transport in amorphous Li_2O_2. *Chem. Mater.* **2014**, *26*, 2952–2959.

[42] Li, J. J.; Han, K.; Huang, J. H.; Li, G. Y.; Peng, S. T.; Li, N.; Wang, J. C.; Zhang, W. B.; Du, Y.; Fan, Y. Q. et al. Polarized nucleation and efficient decomposition of Li_2O_2 for Ti_2C MXene cathode catalyst under a mixed surface condition in lithium-oxygen batteries. *Energy Storage Mater.* **2021**, *35*, 669–678.

[43] Kim, G.; Liu, T.; Temprano, I.; Petrucco, E. A.; Barrow, N.; Grey, C. P. Cycling non-aqueous lithium-air batteries with dimethyl sulfoxide and sulfolane co-solvent: Evaluating influence of sulfolane on cell chemistry. *Johnson Matthey Technol. Rev.* **2018**, *62*, 332–340.

[44] Burke, C. M.; Pande, V.; Khetan, A.; Viswanathan, V.; McCloskey, B. D. Enhancing electrochemical intermediate solvation through electrolyte anion selection to increase nonaqueous Li-O_2 battery capacity. *Proc. Natl. Acad. Sci. U S A* **2015**, *112*, 9293–9298.

[45] Ma, T.; Ni, Y. X.; Wang, Q. R.; Zhang, W. J.; Jin, S.; Zheng, S. B.; Yang, X.; Hou, Y. P.; Tao, Z. L.; Chen, J. Optimize lithium deposition at low temperature by weakly solvating power solvent. *Angew. Chem., Int. Ed.* **2022**, *61*, 202207927.

[46] Erlich, R. H.; Popov, A. I. Spectroscopic studies of ionic solvation. X. Study of the solvation of sodium ions in nonaqueous solvents by sodium-23 nuclear magnetic resonance. *J. Am. Chem. Soc.* **1971**, *93*, 5620–5623.

[47] Johnson, L.; Li, C. M.; Liu, Z.; Chen, Y. H.; Freunberger, S. A.; Ashok, P. C.; Praveen, B. B.; Dholakia, K.; Tarascon, J. M.; Bruce, P. G. The role of LiO_2 solubility in O_2 reduction in aprotic solvents and its consequences for Li-O_2 batteries. *Nat. Chem.* **2014**, *6*, 1091–1099.

[48] Prehal, C.; Mondal, S.; Lovicar, L.; Freunberger, S. A. Exclusive solution discharge in Li-O_2 batteries. *ACS Energy Lett.* **2022**, *7*, 3112–3119.

[49] Schroeder, M. A.; Pearse, A. J.; Kozen, A. C.; Chen, X. Y.; Gregorczyk, K.; Han, X. G.; Cao, A. Y.; Hu, L. B.; Lee, S. B.; Rubloff, G. W. et al. Investigation of the cathode–catalyst–electrolyte interface in aprotic Li-O_2 batteries. *Chem. Mater.* **2015**, *27*, 5305–5313.

[50] Zhou, H. M.; Guo, L.; Zhang, R. H.; Xie, L.; Qiu, Y.; Zhang, G. L.; Guo, Z. H.; Kong, B.; Dang, F. Precise engineering of octahedron-induced subcrystalline $CoMoO_4$ cathode catalyst for high-performance Li-air batteries. *Adv. Funct. Mater.* **2023**, *33*, 2304154.

[51] Qiu, Y.; Li, G. Y.; Zhou, H. M.; Zhang, G. L.; Guo, L.; Guo, Z. H.; Yang, R. N.; Fan, Y. Q.; Wang, W. L.; Du, Y. et al. Highly stable garnet $Fe_2Mo_3O_{12}$ cathode boosts the lithium-air battery performance featuring a polyhedral framework and cationic vacancy concentrated surface. *Adv. Sci.* **2023**, *10*, 2300482.